International Journal of Thermophysics, Vol. 26, No. 4, July 2005 (© 2005)
DOI: 10.1007/s10765-005-6687-7

Material Effect and Steam Explosion at High Temperature ($T > 2300$ K)[1]

P. Piluso,[2,3] G. Trillon,[2] and D. Magallon[2,4]

In the frame of nuclear power plant safety, the interaction of molten corium (mixture of materials coming from a power plant) with water can generate dynamic loading of the surrounding structures. This phenomenon is called the steam explosion. Many experiments have been performed in the KROTOS facility with simulation materials (Al_2O_3) and prototypical materials ($(U,Zr)O_2$, and different behaviors attributed to a 'material effect' have been observed. Alumina melts produced spontaneous energetic steam explosions, whereas explosions with corium melts (80% UO_2–20% ZrO_2) must be triggered and are less energetic. These differences may be partly attributed to the formation of meta-stable gamma alumina and the ability of liquid alumina to dissolve part of the water, acting like an internal trigger. These results mean that alumina is probably not an adequate simulation of the corium for steam explosion.

KEY WORDS: alumina; corium; high temperature; material effect; steam-explosion; trigger.

1. INTRODUCTION

In the framework of nuclear power plant safety, an important issue in case of severe accident is steam explosion; this event could occur during the interaction between the 'corium' (molten mixture of the nuclear power

[1] Paper presented at the Seventh International Workshop on Subsecond Thermophysics, October 6–8, 2004, Orléans, France.

[2] Commissariat à l'Energie Atomique, CEA-Cadarache, Direction de l'Energie Nucléaire, Laboratoire d'essai pour la Maîtrise des Accidents Graves, Bâtiment 708, 13108 St. Paul lès Durance Cédex, France.

[3] To whom correspondence should be addressed. E-mail: pascal.piluso@cea.fr

[4] European Commission, Joint Research Centre-Energy Institute, Petten, The Netherlands.

plant components) and the water generating dynamic loading of the surrounding structures. During this very short interaction, phenomena involving thermal-hydraulic and physico-chemistry mechanisms take place at the millisecond time scale.

A series of global high-temperature experiments ($T > 2300\,\mathrm{K}$) has been conducted at the European Centre JRC/Ispra with simulation materials (Al_2O_3) and power plant materials ($U_{1-x}Zr_xO_2$, $x = 0.2$) in the KROTOS facility to study steam explosion. The latter could melt up to 6 kg of materials which were injected into a 1-m deep water pool. Important differences have been noted between the materials with respect to their propensity to induce steam explosion and to the yields obtained. This gave rise to numerous investigations on the possible causes for these differences, for which existing steam explosion codes can hardly reproduce. One direction of investigation is the role of the thermophysical properties, the so-called 'material effect.'

Actually, although many numerical models and codes have been developed for more than 15 years, none of them consider all the aspects of this material effect (e.g., physico-chemistry). In this paper, we describe the four phases of a steam explosion, the main known mechanisms and the main poorly understood phenomena. Finally, we present new results based on recent characterization of an alumina debris KROTOS experiment, which allowed us to identify mechanisms that may play a significant role in explaining steam explosion behavior.

2. STEAM EXPLOSION EVENT IN A NUCLEAR POWER PLANT

2.1. Severe Accidents in a Nuclear Power Plant

Safety studies are required under accident and severe accident conditions for current and future water-cooled nuclear power plants. In a hypothetical case of a core melt-down in pressurized water power plants (PWR), severe accident scenarios must be considered; the core cooling systems could fail and a very high temperature would be reached (up to 3300 K). In this case, the materials of the nuclear power plant (nuclear fuel, cladding, metallic alloys, structural materials, concrete, etc.,) could melt to form complex and aggressive mixtures called corium.

In this context, the French Atomic Energy Commission (CEA) has been pursuing a large R&D programme on nuclear severe accidents for many years [1–3]. An understanding of the corium behavior in the various phases envisioned for severe accidents is a key aspect required for improving power plant safety. It encompasses the development of models and codes, performance of experiments in simulation, and prototypical materials.

The CEA severe accident R&D studies on corium behavior address the following topics: molten core concrete interaction (MCCI), molten fuel coolant interaction (MFCI), in vessel retention with power plant pit flooding, and corium–ceramic interaction. The experiments with prototypical corium (i.e., material containing depleted UO_2) are performed in the PLINIUS experimental platform at CEA Cadarache [4].

For the safety analysis of severe accidents in a nuclear power plant, the MFCI is considered because in this case a 'steam explosion' could occur and contribute to power plant vessel failure and a possible failure of the containment with release of radioactive fission products [5].

2.2. Main Mechanisms of the Steam Explosion

The steam explosion in a nuclear power plant is the physical event in which a hot melt (corium) is quickly fragmented and its internal energy is transferred to a colder more volatile liquid (the coolant, i.e., the water) [6]. The consequences are the quick vaporization of the water at high pressure and an energetic thermal detonation.

The steam explosion can be decomposed into four phases considering the case of the configuration of the melt penetration in water (see Fig. 1) [6].

2.2.1. First Phase: Pre-mixing Between the Corium and the Water — Coarse Fragmentation [6, 7]:

In a first approach, the pre-mixing can be qualitatively described like a dispersion of corium in the liquid state and the coolant in the liquid state within one another (e.g., discrete corium liquid surrounded by continuous coolant liquid). More precisely, during the penetration of the melt into water, the hydrodynamic forces induce fragmentation of the melt into single particles of cm size. The result is, first of all, a coarse fragmentation or melt break-up. The particles fragment, in turn, into smaller particles until they reach a critical size such that the cohesive forces (surface tension) balance exactly the disruptive forces (inertial). The typical picture is that of a melt jet descending in a water pool and decreasing in diameter due to this break-up process. Depending on the initial diameter of the jet and on the water pool depth, the jet column might be completely eroded or not at the bottom, and we get an axial distribution of particle sizes ranging from cm to mm size mixed with water (see Fig. 2). This phase is characterized by a steam production rate at a time scale of the same order as the time scale of the melt pouring rate. The difference between the boiling temperature of the water and the corium temperature is so high that the boiling regime of the water is always film boiling

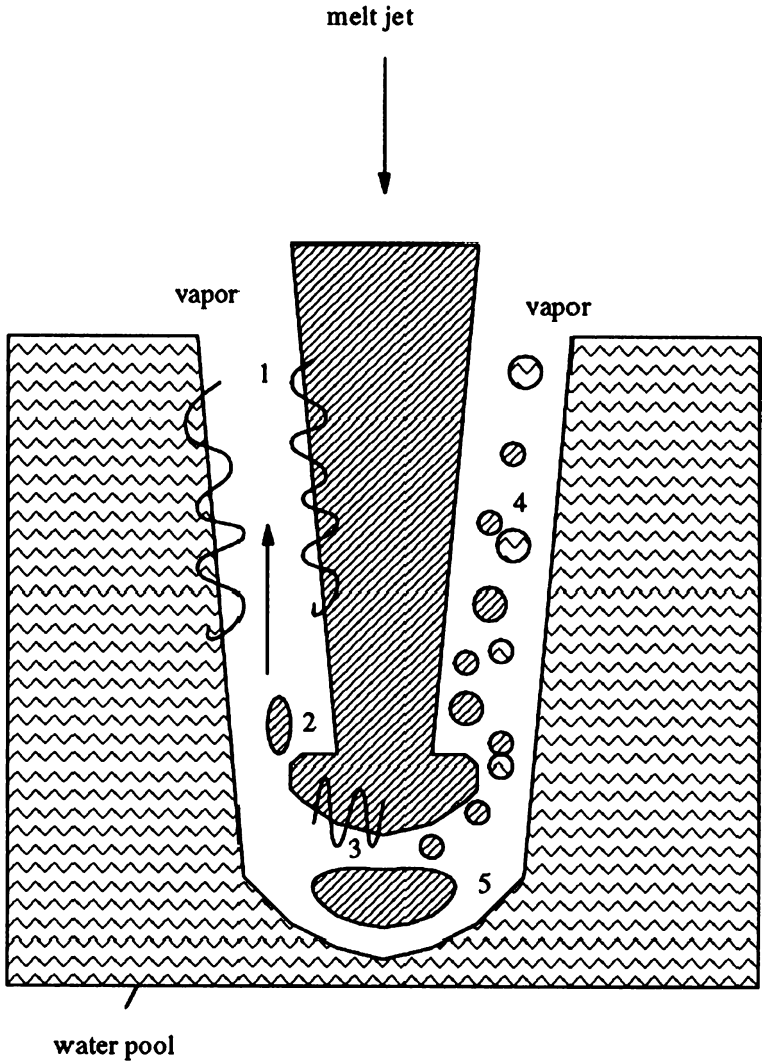

Fig. 1. Phenomena involved in a jet break-up.

in the power plant condition. This allows mixing of a large quantity of corium with water, the corium remaining in the molten state and transferring little energy to the water. It results in a slow pressurization of the system, or even not, if condensation is able to balance vaporization. In film boiling, this situation is unstable, but the degree of instability depends

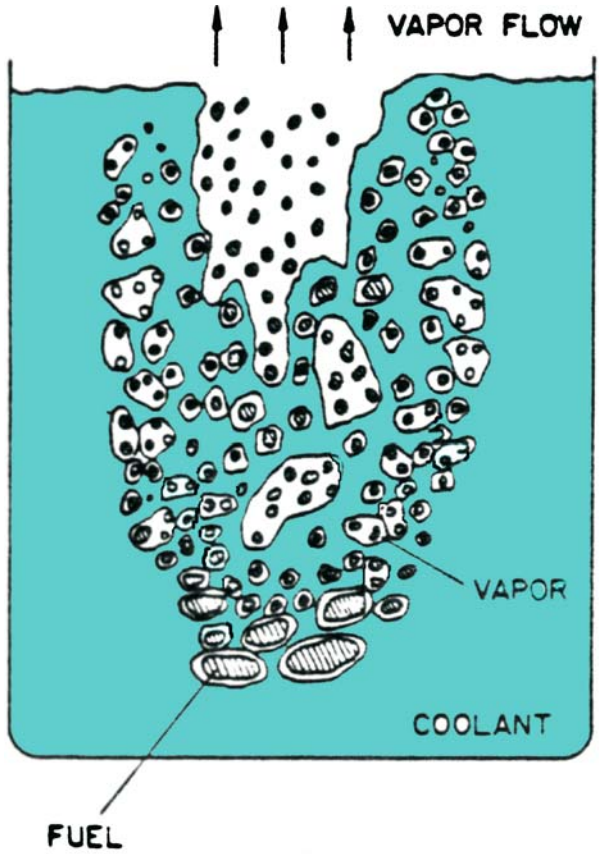

Fig. 2. Possible mixing configuration (corium/coolant) [6].

on the system and on the conditions. It can last as long as the melt is available, thus resulting in a debris bed on the collecting structure (case of the severe accident which occurred in 1979 in the industrial nuclear power plant TMI-2-Pennsylvania-USA).

2.2.2. Second Phase: Triggering and Fine Local Fuel Fragmentation [5–7]

Most fuel–coolant interactions appear to be initiated by the collapse of the vapor film layer or the bubble in a local region. If a local perturbation is introduced in the system such as to induce a local explosion somewhere, it may propagate into the pre-mixture and result in an explosion involving all the melt in flight in the water at that time (and maybe more). In this case, the perturbation is the *trigger* of the explosion, which can be

internal to the system (spontaneous) or *external* (artificially or accidentally induced).

- *For an external trigger*, a pressure pulse of a certain duration and a certain amplitude generated by the sudden rupture of a high-pressure gas capsule or a small chemical explosion is able to trigger a propagating event in experiments [5].
- *For an internal trigger,* the origins and the possible explanations are less clear.

Transition to transition or nucleate boiling upon mixture contact with steel surrounding structures is supposed to be one possible mechanism capable to trigger an explosion. For the triggering mechanisms and the destabilization of the steam film boiling process, many studies have been done since the 1970s. Among the seven classes of film boiling proposed by Walford [8], the explosive cavity is one possible triggering mode. It can be represented as a sphere (liquid corium) in a spherical cavity (steam film); the sphere is going to progress through the cavity until the sphere nears the steam–liquid interface when another cavity is rapidly formed. The repetition of the cycle is about 5 to 10 μs. Steven and Witte [9] proposed two types of behavior for the destabilization steam film: a precipitous instability, referred to as a 'transplosion,' and a progressive instability controlled by bubble-like irregularities on the liquid–steam interface. Kim and Corradini [10] argued that the oscillatory behavior of the steam film is responsible for the fuel–coolant interaction; higher oscillation and pressure fluctuation of the steam film will facilitate the triggering of the fuel–coolant interaction (see Fig. 3).

2.2.3. Third Phase: Propagation [5]

This is the process by which thermal energy of the melt is converted into thermal energy in the coolant. The fragmentation propagates at a velocity which depends on the conditions in the pre-mixing region. It can be governed by time scales corresponding to the propagation of disturbances in the pre-mixing region, resulting in sequential ignition of the mixture. Typical velocities in this case are of the order of some *tens of* $\mathrm{m \cdot s^{-1}}$. In this case, the pressurization of the system is relatively limited, slow and uniform, without generation of shock waves. Nevertheless, it can escalate up to reaching *supersonic velocities* in the pre-mixture and quasi-steady-state propagation. For example, velocities in excess of $1000\,\mathrm{m \cdot s^{-1}}$ have been measured in Al_2O_3–water systems. Depending on conditions, the pre-mixture can 'burn' more or less completely before the system can expand, creating a zone of high pressure. If conditions are favorable (e.g.,

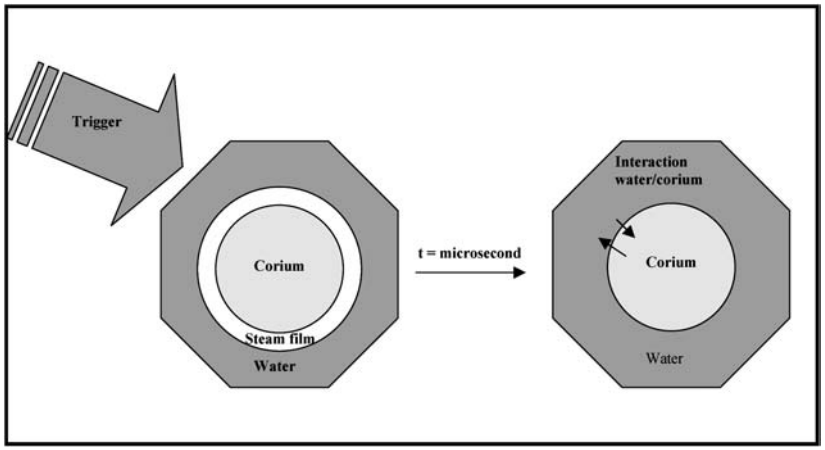

Fig. 3. General scheme for the destabilization of the steam film around a corium droplet.

1-D with trigger at one end), all the pre-mixture can burn before any expansion can take place: supercritical explosions with dynamic pressures of the order of 100 MPa and impulses in excess of 100 kPa · s have been obtained in Al_2O_3–water systems in quasi-1-D configurations [11].

2.2.4. Fourth Phase: Expansion [5]

The expansion phase is the phase when the thermal energy in the coolant is converted into mechanical energy. The pressure relief through shock waves can be the cause of direct damage to the surrounding structures or generate a water slug, which eventually transfers its kinetic energy to the structures. There is the risk that the containment can lose its integrity if a steam explosion occurs in a flooded cavity during the melt relocation.

Board et al. [11] have proposed a conceptual approach of a "thermal detonation" by analogy with chemical detonation (see Fig. 4). The thermal detonation can be divided into four zones:

1. the mixing zone: undisturbed region where film boiling conditions prevail.
2. the fragmentation zone: a shock induces the film collapse and differential velocities between melt and coolant, which causes

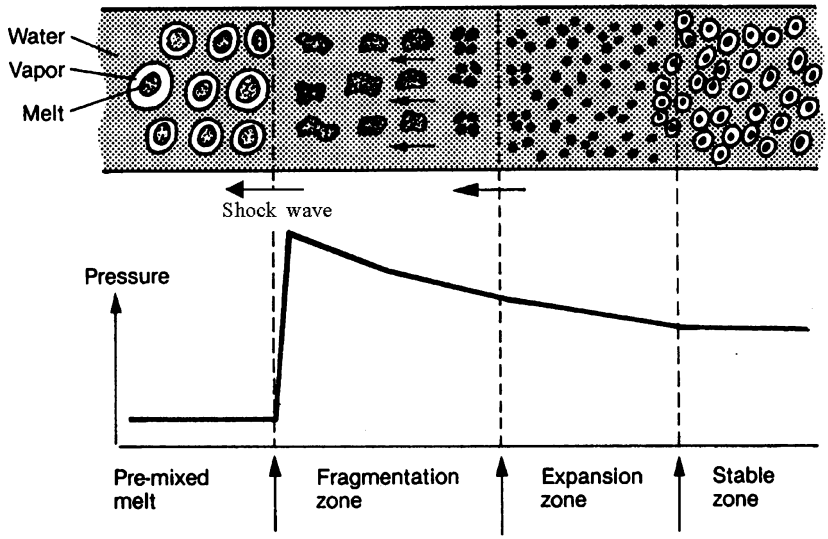

Fig. 4. Conceptual picture of a thermal detonation [12].

hydrodynamic fragmentation of the melt and thermal fragmentation. Both results in fine fragmentation of the melt and extensive heat transfer to the water.

3. the expansion zone: high pressure region which, by expanding, drives the front forward.
4. the stable zone: region where the velocities have returned to zero.

3. FACILITY DEVOTED TO STEAM EXPLOSION INVESTIGATION: KROTOS

3.1. Description of the KROTOS Facility

The KROTOS facility at the European Centre JRC/Ispra was devoted to experimental studies of steam explosion according to various conditions [11,13–15]:

- materials: pure simulation compounds (NaCl, Sn, Al_2O_3) and nuclear power plant mixtures ($U_{1-x}Zr_xO_2$)
- masses: 1 to 6 kg
- maximum achievable temperatures in the furnace: about 3300 K
- spontaneous explosion: trigger, spontaneous

- design of KROTOS vessel: 4.0 MPa at 493 K
- water: saturated, nonsaturated.

The KROTOS test facility (see Fig. 5) consists mainly of a radiation furnace, a release line, and the test vessel section. The furnace includes a cylindrical tungsten heater element which encloses the crucible containing the melt material [11]. The crucible is held in place by means of a pneumatically operated release hook. Eight concentric tungsten, molybdenum, and steel radiation shields are radially placed around the heater element. The top and bottom parts of the heated zone are insulated with thermal screens to reduce heat losses to the surroundings. The furnace is covered with a bell-shaped, water-cooled lid designed either to operate under vacuum conditions or to withstand 0.3 MPa overpressure (He). The three-phase electric power supply has a maximum power of 130 kW. The melt temperature is controlled by an optical bi-chromatic pyrometer measuring the wall temperature of the crucible. The lower part of the KROTOS facility [11] consists of a pressure vessel and test section (see Fig. 6), both made of stainless steel. It is a cylindrical vessel of 0.57 m inner diameter and 2.0 m in height (volume: $\sim 0.35\,m^3$) with a flanged flat upper head plate. The test section consists of a strong stainless steel tube with an inner diameter of 200 mm and an outer diameter of 240 mm. The water level is variable up to about 1.3 m.

After reaching the desired melt temperature [11], the crucible containing the melt is released from the furnace and falls by gravity through an ~ 5.2-m long release tube. Half-way down the tube, a fast isolation valve separates the furnace from the test section below. During its fall, the crucible cuts a copper wire, which sends a signal to close the isolation valve and generates a zero time signal for the data acquisition. Finally, the crucible strikes a retainer ring at the end of the tube where a conical-shaped spike pierces the bottom of the crucible and penetrates into the melt allowing the melt to pour out through the openings in the puncher. The melt arrival is detected by sacrificial thermocouples and by a high-speed video camera (NAC) mounted in the upper view port of the test vessel (Fig. 5). If the gas trigger device is used, it is activated by a time-delay circuit when the melt arrives at the desired mixing depth. Dynamic pressures during the melt–water interaction are measured using piezoelectric transducers. These pressure measurements also allow estimation of the starting location of the explosion and propagation speed, which are important for modeling. The integral void fraction during mixing is determined by measuring the water level in the test section at two locations and averaging. Measurements of vessel pressurization [11] with sensors designated as C1–C3 in Fig. 6 help to determine the steaming rates and

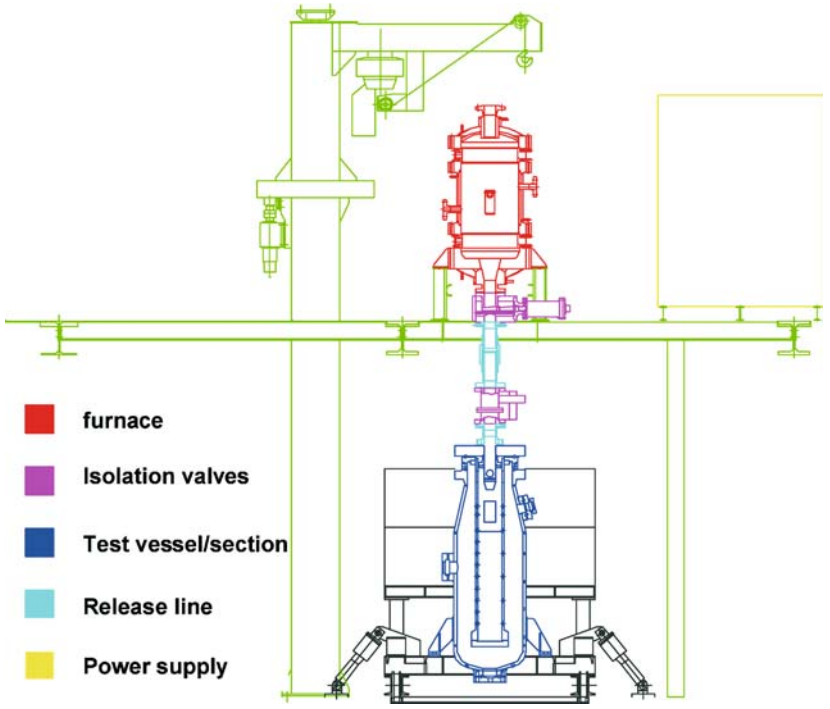

Fig. 5. KROTOS test facility.

possible pressurization due to hydrogen production during mixing, and also permit calculation of the steam explosion expansion work.

3.2. KROTOS-Alumina Experiments

More than 50 experiments have been performed through 1999 at JRC/Ispra (Italy) in the KROTOS facility using various experimental conditions [11, 13–15].

We will focus on the KROTOS-alumina experiments. The initial alumina was pure alumina ($> 99.99\%$) without macroscopic defects (gas bubbles). The same experimental conditions have been applied for the fusion stage: He atmosphere, molybdenum or tungsten crucible, $P = 1.2$ bar, heating rate: $2000^{\circ}\mathrm{C} \cdot \mathrm{h}^{-1}$, overheating/melting point: $150^{\circ}\mathrm{C}$. Three KROTOS experiments have been selected:

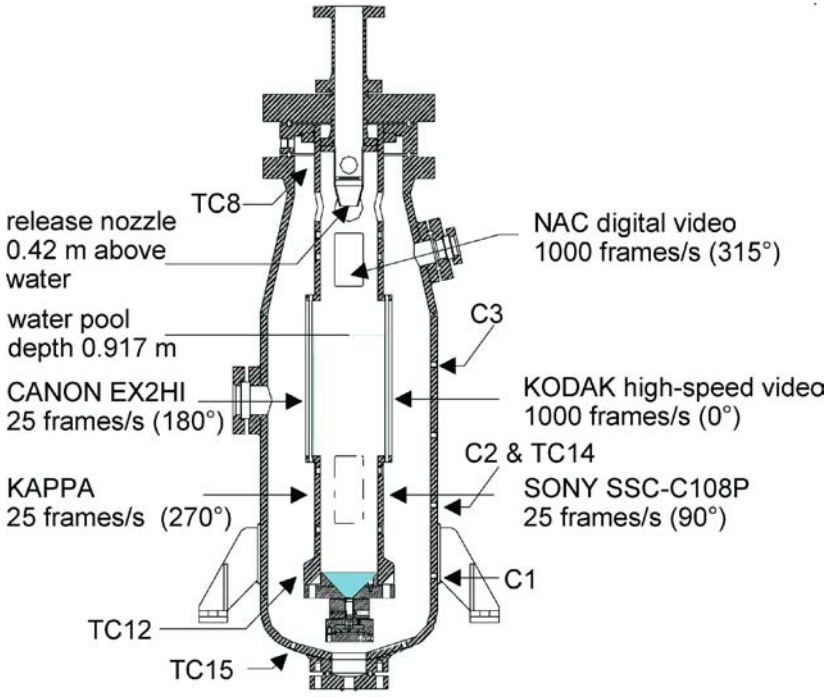

Fig. 6. KROTOS test vessel [11].

- KROTOS M: the alumina has been melted in the crucible.
- KROTOS K-27: the alumina has been melted in the crucible, transferred, and coarse fragmented (see Section 2.2, stage 1 of the steam explosion).
- KROTOS K-49: the alumina has been melted in the crucible, transferred coarse fragmented (see Section 2.2, stage 1 to stage 4 of the steam explosion).

These three experiments have been selected because they are representative of the different stages of the steam explosion, using the melted state as the reference.

Table I summarizes the initial conditions for the KROTOS-alumina experiments and shows as a comparison a standard KROTOS-corium (80 mass% UO_2-20 mass% ZrO_2) after application of an external trigger. Table II presents the main final characteristics of the alumina and corium tests.

Table I. Initial Experimental Conditions for KROTOS-Alumina and KROTOS-Corium Tests

Test		K-M	K-27	K-49	K-58
Melt composition		Al_2O_3	Al_2O_3	Al_2O_3	80 mass% UO_2 20 mass% ZrO_2
Melt mass	(kg)	1.7	1.37	1.47	3.6
Melt temperature	(K)	2400	2350	2688	3077
Melt jet diameter	(mm)	–	30	30	30
Fall height in gas	(m)	–	0.4	0.44	0.42
Water depth	(m)	–	0.112	1.105	0.917
Water mass	(kg)	–	7.2	34.00	30.9
Water temperature	(K)	–	351	294	288
Water subcooling	(K)	–	10	120	125
Initial pressure	(MPa)	–	0.1	0.37	0.37
Freeboard volume	(m^3)	–	0.3	0.23	0.334
Cover gas		–	He	He	He
Gas trigger		–	No	No	Yes
Gas trigger pressure	(MPa)	–	–	–	15
Gas trigger energy	(J)	–	–	–	695

Table II. Main Experimental Results for KROTOS-Alumina and KROTOS-Corium Tests

Test		K-M	K-27	K-49	K-58
Melt composition		Al_2O_3	Al_2O_3	Al_2O_3	80 mass% UO_2 20 mass% ZrO_2
Explosion pressure	(MPa)	–	–	127	25.8
Total debris	(kg)	–	1.1	–	3.6
Coarse debris (> 1 mm)		–	60% > 12 mm	Yes	Yes
Fine debris (< 1 mm)		–	No	Yes (Mean diameter: 0.250 mm)	Yes (Mean diameter: 0.177 mm)

3.3. Post-Test Characterization of KROTOS-Alumina Experiments

Samples representative of the KROTOS experiments (M, K27, K49, see Section 3) have been taken and post-test-characterized. Different types of post-test analyses were performed on those samples: visual observations, geometric and volume analyses, optical microscopy, scanning electron microscopy coupled with X-ray analysis, and X-ray diffraction (XRD). We will focus the discussion on XRD analysis, i.e., identification of the crystallographic phases after steam explosion. The diffractometer

used to perform these measurements was a Debye–Scherrer-configured diffractometer with a mono-chromator allowing a monochromatic incident X-ray beam, using a curved localization detector INEL CPS 120, and a special nuclearized sample holder. No other treatments rather than single-peak refinements for qualitative analysis have been used. The diffractograms obtained on the three representative samples of KROTOS alumina samples are shown in Fig. 7. The interpretation of the diffractograms and the comparison with the JCPDS powder diffraction file [16] allowed the following phase identifications for the KROTOS-alumina experiments:

- *KROTOS-M*: one phase: the alpha alumina; (corundum) rhomboedric
  Lattice parameters: $a = b = 0.475\,nm$, $c = 1.2991\,nm$.
- *KROTOS-K 27*: one phase: the alpha alumina; (corundum) rhomboedric, the same as KROTOS-M.
  Lattice parameters: $a = b = 0.475\,nm$, $c = 1.2991\,nm$.
- *KROTOS K-49*: the gamma alumina (major phase): cubic phase
  Lattice parameters: $a = b = c = 0.7939\,nm$.

These important post-test characterizations show clearly a difference between the crystallographic phases of the melted and melted/coarse fragmented alumina on the one hand and of the 'exploded' alumina on the other.

4. DISCUSSION

4.1. Is There a Material Effect for Steam Explosion?

The difference in the behavior of ($U_{1-x}Zr_xO_2$) corium mixture melts and alumina melts injected into sub-cooled water have been identified since 1995 [14]. The first important difference concerns the spontaneity of the steam explosion,: alumina melts produced *spontaneous* steam explosions, whereas corium melts fragmented and quenched without steam explosion if any *trigger* has been applied (see Table I). The second important difference concerns the characteristics of the steam explosion [15]: the intensity of the peak pressure, the dynamics of the increase of the pressure, and the energy had always been higher for alumina melt than for corium mixture melts (see Fig. 8). The differences in steam explosion behavior have been attributed to various factors such as *composition of the melt* (physical and chemical properties), *melting/solidification temperature of the melt*, *superheat of the melt, production of non-condensable gases, magnitude of the trigger, etc*. A number of analytical studies were performed to

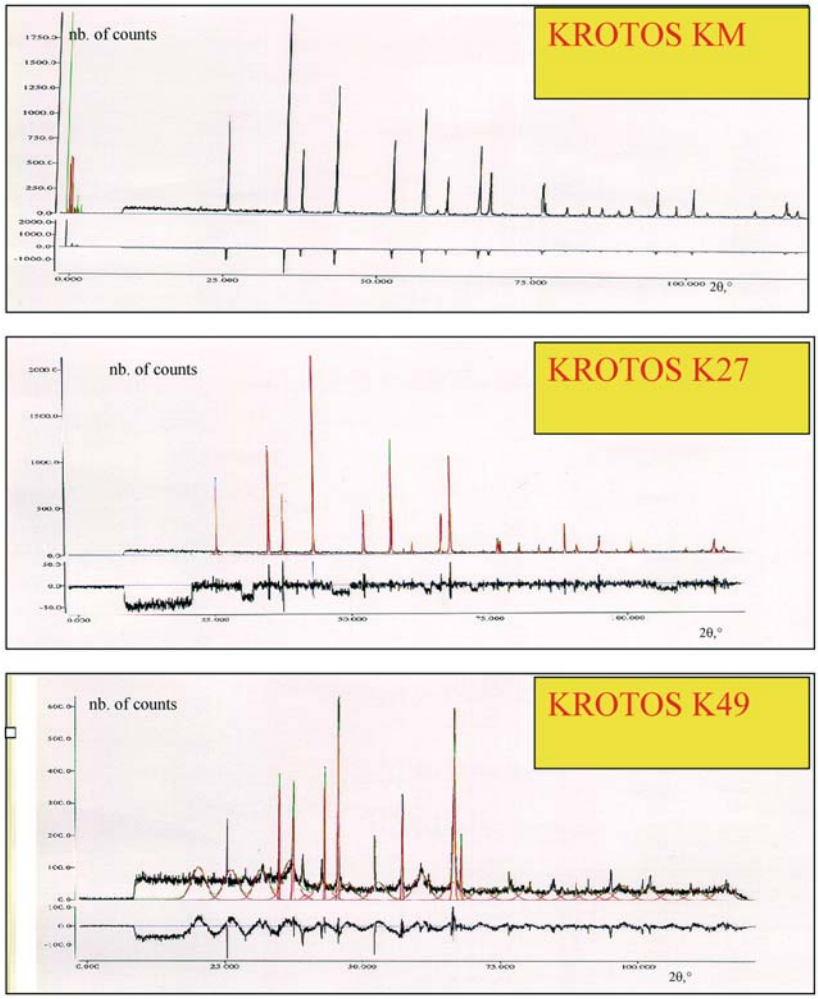

Fig. 7. X-ray diffractograms of KM, K-27, and K-49 KROTOS samples.

directly investigate the influence of those factors, in particular, the characterization of the pre-mixing phase [15]. It has been shown that alumina and corium melts have different pre-mixing behaviors (Fig. 9): the penetration of melt into the water forms a jet with small globules (size about 1 mm, some globules have a hole inside) for the corium mixture, whereas this is a separate jet with coarse globules and chips (size about 12 mm, some globules have a hole inside) for alumina. More generally, a generic

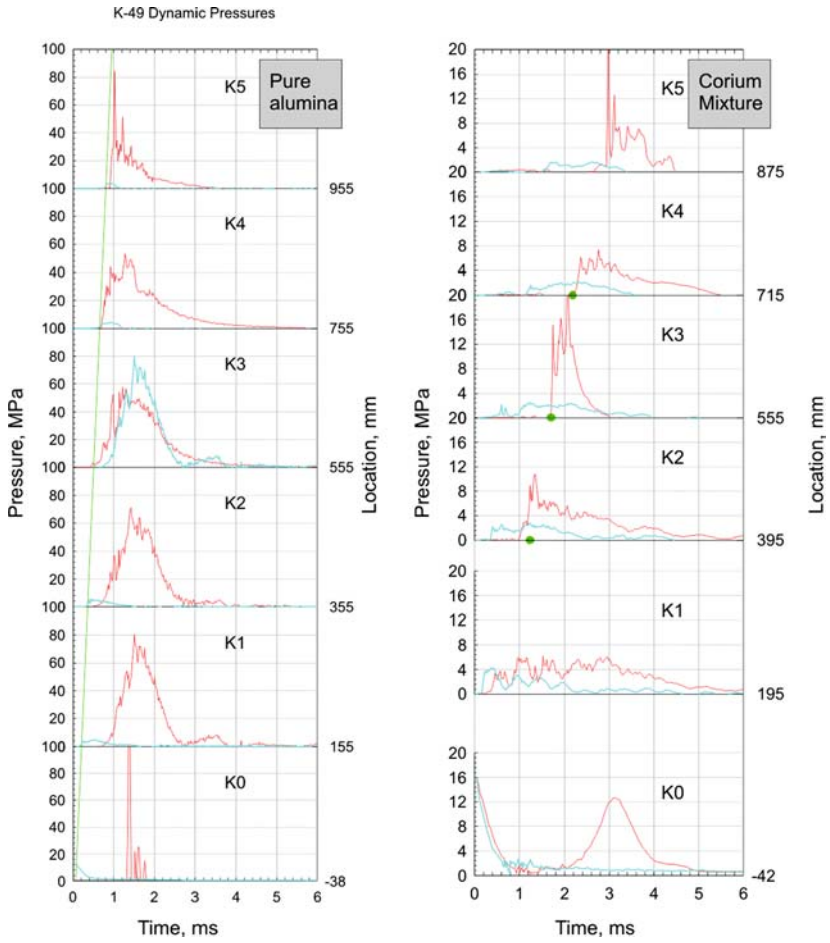

Fig. 8. Comparison of the dynamic explosion pressure between pure alumina (left) and 80 mass % UO_2-20 mass % ZrO_2 corium mixture (right) in KROTOS experiments.

term of 'material effect' has been attributed to explain the differences of behavior between alumina and prototypical corium in steam explosion, but it has not been clearly explained.

4.2. What is Alumina in the Liquid and Solid States?

As has been shown in Section 3.3, there are two different final states between the exploded alumina and the non-exploded alumina. Now, we have to precisely define alpha and gamma alumina.

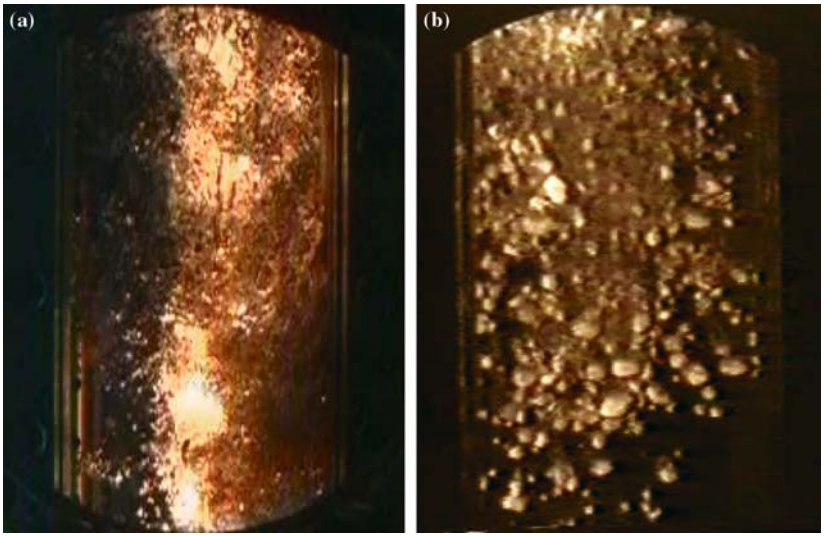

Fig. 9. (a) Corium melt mixing (CANON): viewing area 10 cm by 20 cm and (b) alumina melt mixing (CANON): viewing area 10 cm by 20 cm.

The alpha alumina is the unique crystallographic phase which is *thermodynamically* stable [17]. This alpha alumina has a hexagonal structure (R3C) and the cation Al^{3+} is in octahedral coordinance (two thirds of the sites are occupied).

The gamma alumina is a transition alumina, i.e., a *metastable* phase. Seven known types of transition alumina exist. This gamma alumina has a spinel structure (Fd3-m). The anionic sub-lattice has an order, whereas the cationic sub-lattice has some defects (Vacancies: V). The existence of the defects means that it is necessary to add several per cent of OH^- ions to preserve the electro-neutrality. Some authors [18] have postulated the necessity of the equality between the hydroxyl groups and the cationic vacancies to have a gamma alumina structure. In this case, the gamma alumina can be written as $Al_2V_{0.4}O_{2.8}(OH)_{0.4}$. Another specific point of the gamma alumina concerns the existence of a large specific area (several hundred $m^2 \cdot g^{-1}$). This kind of large specific area means a great surface reactivity, especially easy adsorption of one/two layers of OH^- or H_2O. This phenomenon is reversible.

The alumina in a liquid state is an 'ordered' liquid at short distance (a few atomic rows). AlO_6 octahedron would be the basis ordered structure [19]. The liquid density is estimated at $3010\,kg \cdot m^{-3}$. Alumina in a liquid state can dissolve steam according to some conditions of pressure

and temperature [20]. For those experiments, a solar furnace has been used and the alumina in a liquid state was in a pressurized tank at 390 K. The capability of liquid alumina to dissolve a part of the steam has been estimated according to a general empirical relation in $(p_{H2O})^{0.5}$. An important consequence of the dissolution of the steam in the liquid alumina is the decrease of the viscosity. Another phenomenon occurs during the solidification process: a spitting phenomenon and H_2O and H_2 are liberated in two or three steps related to the intensity of the spitting phenomenon [21]. For the spitting process, 0.47 ± 0.02 mg H_2O per g Al_2O_3 have been measured whereas 0.50 ± 0.05 mg H_2O per g Al_2O_3 in the solid which means that the dissolution process of the steam in the liquid alumina can accept about 1 mg H_2O per g Al_2O_3.

4.3. Possible Explanation for the Final State of the KROTOS-Alumina Experiments

The ability for alumina in a liquid state to dissolve steam must be taken into account as a possible 'internal' trigger to initiate the steam explosion under specific conditions of temperature and pressure of the water. The absorption of the steam film in the volumetric alumina droplet could facilitate direct contact between alumina and water and so participate in the triggerability explaining in part the 'spontaneity' of (KROTOS K-49) in comparison with prototypical corium (KROTOS K-58). This possible interpretation is emphasized by the post-test characterization of KROTOS-alumina experiments: KROTOS K-49 (steam explosion) consists mainly of gamma alumina, i.e. as $Al_2V_{0.4}O_{2.8}(OH)_{0.4}$, evidence of the volumetric absorption of H_2O, whereas KROTOS K-27 (non-explosion) consists mainly of alpha alumina (without water). Nevertheless, it must be noted that the beginning of the alumina steam explosion has been observed when the melt was in contact with *the walls* of the vessel and not when the melt was introduced *into the water*. This delay, if the volumetric absorption of the water participates as the trigger, is not yet well explained.

Another effect must be taken into account during the solidification of the alumina: the release of water and hydrogen (non-condensable gas), this last one being a limitation factor in steam explosion.

Usually, gamma alumina is associated with a large specific area ($> 100\,m^2 \cdot g^{-1}$). Such a large specific area could drastically reduce the time for energy transfer to the coolant and thus increase energetics which is generally not taken into account in debris analyses (sieving method).

A last point concerns the metastability of alumina experiments. The existence of a metastable alumina means that the alumina solidification

path (KROTOS K-49) was out of equilibrium and some kinetic factors must be taken into account in the classical steps of nucleation/germination/growth of the stable phase. The nucleation rate is determined by the nucleation energetic barrier ΔG*. For the solidification of individual droplets, it is well known [22] that the homogeneous nucleation occurs below the equilibrium solidification temperature ($T_m = 2330$ K). Usually, only a small part of the droplets are going to solidify at T_m. At steady state, the nucleation rate is given by

$$I = A\exp(-\Delta G*/\mathrm{k}T)$$

where I is the nucleation rate, k is Boltzmann's constant, A is a constant, and ΔG* is the critical free energy for nucleation;

$$\Delta G* = K\gamma^3 T_f^2/\Delta H_m^2 \Delta T^2$$

where γ is the interfacial surface energy, K is a nucleus form factor, ΔH_m is the melting enthalpy, and ΔT is the undercooling.

The undercooling increases when the particle size decreases because the probability to find an active site is lower [23]. For particle sizes between 100 and 10 μm, the under-cooling can impose a solidification temperature of 0.82 T_m which means for the KROTOS-K49, a solidification temperature of 1910 K whereas 2330 K was considered. This parameter may act on the liquid fraction available during steam explosion propagation.

5. CONCLUSION

For many years, numerous studies in the field of nuclear power plant safety have been leading to a better understanding of an important remaining issue: the steam explosion. This phenomenon is very complex and involves different fields of science: thermal-hydraulics, physics, and chemistry. A still open question is the existence of a 'material effect' and the differences of behavior between a simulation material (alumina) and the prototypical material (corium). The differences of behavior in steam explosions have been attributed to various factors such as composition of the melt (physical and chemical properties), melting/solidification temperature of the melt, superheating of the melt, production of non-condensable gases, and magnitude of the trigger.

For the KROTOS-alumina experiments, a different alumina crystallographic structure for the final states between the exploded alumina (formation of meta-stable gamma alumina) and the non-exploded alumina

(formation of the stable alpha alumina) has been demonstrated. This existence of the gamma alumina means a volumetric absorption of H_2O with a general formulation such as $Al_2V_{0.4}O_{2.8}(OH)_{0.4}$, whereas the existence of the alpha alumina means a phase without H_2O.

The ability for alumina in a liquid state to dissolve steam could be taken into account as an 'internal' trigger and could participate as a catalyzer to initiate the steam explosion under specific conditions of temperature and pressure and water. In this case, the steam film could be partly or totally absorbed in the alumina droplet and direct contact between alumina and water could be facilitated that means a direct influence on *the magnitude of the spontaneous trigger*. The absorption of water in the alumina means also modification of some *thermo-physical properties* of the alumina such as viscosity. Finally, the formation of metastable phases, like gamma alumina, could lower the *solidification temperature* of alumina from 2330 to 1910 K and the final size of such gamma alumina is about a few nm, whereas the modeling and the calculation codes of the steam explosion give currently a value of 2330 K for the solidification temperature of alumina and a mean size of 250 μm for the fine fragments. In conclusion, it must be emphasized that alumina is probably not a good simulation material of the corium materials for the studies of steam explosion in a nuclear power plant because alumina has a specific behavior that is probably far from the $(U,Zr)O_2$ mixtures.

It must be mentioned that recent experiments have shown spontaneous explosion with a prototypical mixture (70 mass% UO_2-30 mass% ZrO_2) [23] whereas the corium mixture that had been triggered in the KROTOS facility was always 80 mass% UO_2-20 mass% ZrO_2 mixture. At the current state of the art for steam explosion understanding, it is not possible to find a simulation material which could simulate adequately prototypical corium.

In the future, it is planned to perform new experiments at Cadarache with the KROTOS facility. Specific attention will be given to the post-test characterization of the final fragments (fine and coarse), with or without steam explosion to determine if such meta-stable phases $(UO_x\ (OH)_y)$ or $(U,ZrOx_2\ (OH)_y)$ could exist with prototypical materials and what is their importance in the steam explosion.

REFERENCES

1. G. Cognet, G. Laffont, C. Jegou, J. Pierre, C. Journeau, M. Cranga, and F. Sudreau, *OECD Workshop on Ex-Vessel Debris Coolability* (Karlsruhe, Germany, November 15–18,1999), pp. 156–158.

2. G. Cognet, J. M. Seiler, I. Szabo, J. C. Latché, B. Spindler, and J. M. Humbert, *Rev. Gén. Nucl*. **1**:38 (1997).
3. G. Cognet, J. M. Veteau, P. Eberle, and J. M. Seiler, *Nuthos –5 Meeting* (Beijing, China, 1997), pp. 5-1–5-8.
4. P. Piluso, C. Journeau, E. Boccaccio, J. M. Bonnet, P. Fouquart, J. F. Haquet, C. Jégou, and D. Magallon, *Proc. Nuclear Energy for New Europe* (Kranjska Gora, Slovenia, 2002).
5. D. Magallon, I. Huhtiniemi, P. Dietrich, G. Berthoud, M. Valette, W. Schütz, H. Jacobs, N. Kolev, G. Graziosi, R. Seghal, M. Bürger, M. Buck, E. V. Berg, G. Colombo, B. Turland, G. Dobson, and D. Monhardt, *MFCI Project – Final Report* (4th Europ. Framework Programme, EUR, Contract-CT9292-004, 2000).
6. M. L. Corradini, B. J. Kim, and M. D. Oh, *Proc. Nucl. Energy* **22**:1 (1988).
7. A. W. Cronemberg and G. R. Benz, *NUREG/CR-0245, TREE-1242* (1978).
8. F. J. Walford, *Int. J. Heat Mass Tran*. **12**:1621 (1969).
9. L. C. Steven and L. C. Witte, *Int. J. Heat Mass Trans*. **16**:669 (1973).
10. B. Kim and M. L Corradini, *Fifth Int. Meeting on Thermal Nuclear POWER PLANT* (Karlsruhe, Germany, 1984).
11. S. J. Board, R. W. Hall, and R. S. Hall, *Nature* **254**:319 (1975).
12. H. Hohmann, D. Magallon, H. Schins, and A. Yerkess, *Nucl. Eng. Des*. **155**:391(1995).
13. I. Huhtiniemi, D. Magallon, and H. Hohman, *Nucl. Eng. Des*. **189**:379 (1999).
14. I. Huhtiniemi, H. Hohmann, and D. Magallon, *Proc. OECD/CSNI Specialist Meeting on Fuel-Coolant Interaction* (Tokai-Mura, Japan, 1997).
15. I. Huhtiniemi and D. Magallon, *Nucl. Eng. Des*. **204**:391 (2001).
16. *Powder Diffraction File Search Manual* (Fink), Inorganic Phases – International Centre for Diffraction Data (1982).
17. K. Welfers, "Oxides and Hydroxides of Aluminum," *Alcoa Technical Paper No. 19* (Alcoa Lab, 1987).
18. S. Soled, *J. Catal*. **81**:252 (1983).
19. B. Glorieux, *Mesure de la densité, de la tension de surface et de la viscosité de l'alumine liquide en fonction de la température et de l'environnement* (Thèse de l'Université d'Orléans, France, 2000).
20. J. P. Coutures, J. M. Dechauvelle, R. Munoz, and G. Urbain, *Rev. Int. Hautes Temp. Refract*. **17**:351 (1980).
21. R. McPherson, *J. Mat. Sci*. **8**:851 (1973).
22. V. Jarayam and C. G. Levi, *Acta Metall*. **37**:569 (1989).
23. J. H. Kim, I. K. Park, B. T. Min, S. W. Hong, Y. S. Shin, J. H. Song, and H. D. Kim, *Proc. ICAPP '04* (Pittsburgh, Pennsylvania, June 13–17, 2004).